1 **Supporting Information**
2
3 **Deciphering polymer degradation chemistry via integrating novel database construction**
4 **into nontarget analysis**
5

6 Phoebe Keyes[1], Noor Halimah[1], Boya Xiong[1]
7 [1] Department of Civil, Environmental, and Geo-Engineering, University of Minnesota

8
9 _Detection of features in homologue series_
10   Homologue series compounds were detected by searching for triplicate features for which
11 the calculated molecular weight had a mass difference of the acrylamide monomer (71.03114 Da)
12 or a multiple of this. A 5-ppm error was allowed for these comparisons.
13   To create the Kendrick mass defect plots, the Kendrick ratio (R) for acrylamide was
14 calculated.

$$R = \frac{Nominal\ Monomer\ Mass}{Monomer\ Mass}$$

15   **(Equation 1)**
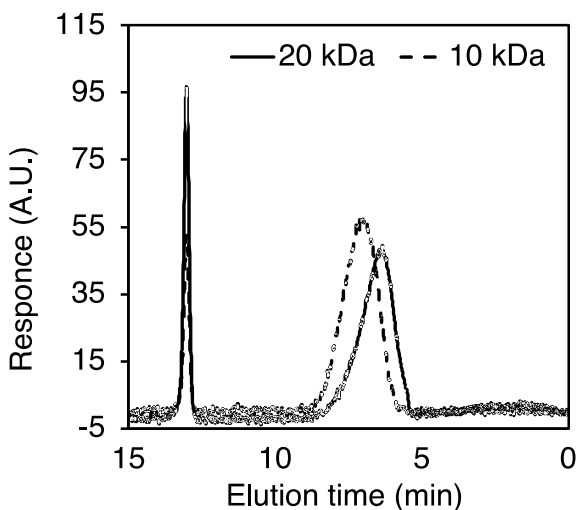16 This value, R was used to calculate the Kendrick mass of each feature.
17 $Kendrick\ Mass = MW \times R$ **(Equation 2)**
18 Finally, the Kendrick Mass Defect (KMD) was calculated for each feature.
19 $KMD = Nominal\ Mass\ of\ Feature - Kendrick\ Mass$ **(Equation 3)**
20 The KMD was then plotted against the MW of all features to get a KMD plot.
21
22 _Polymer standard SEC analysis_
23

24
25 **Figure S1.** The SEC trace of the 20 kDa (solid line) and 10 kDa (dotted line) polymer standard
26 material from the American Polymer Standards (5 g/L). The low molecular weight peak persisted
27 in the SEC trace of different polymer standard solutions, suggesting the lower MW peak was non-
28 PAM features.
29
30 _Dialysis test to examine the nature of the low MW features._
31   A 5 g/L polyacrylamide (PAM) solution was prepared by dissolving PAM (10,000 g/mol,
32 50% w/w in water, Sigma Aldrich, MO) in MilliQ water for 24 h under magnetic stirring. The 30

33 mL of solution was added to a 3.5 kDa dialysis bag (Spectra/Por 3 Dialysis Membrane Standard
34 RC Tubing, Fisher Scientific, NH). This bag was suspended in 5 L of milliQ water for 72 h with
35 magnetic stirring in the milliQ water. Non-purgeable organic carbon (NPOC) measurements were
36 taken on TOC-V series organic carbon analyzer (Shimadzu, Japan). The samples before and after
37 dialysis were analyzed for NPOC (**Fig. S2A**) and molecular weight profile via SEC (**Fig. S2B**).
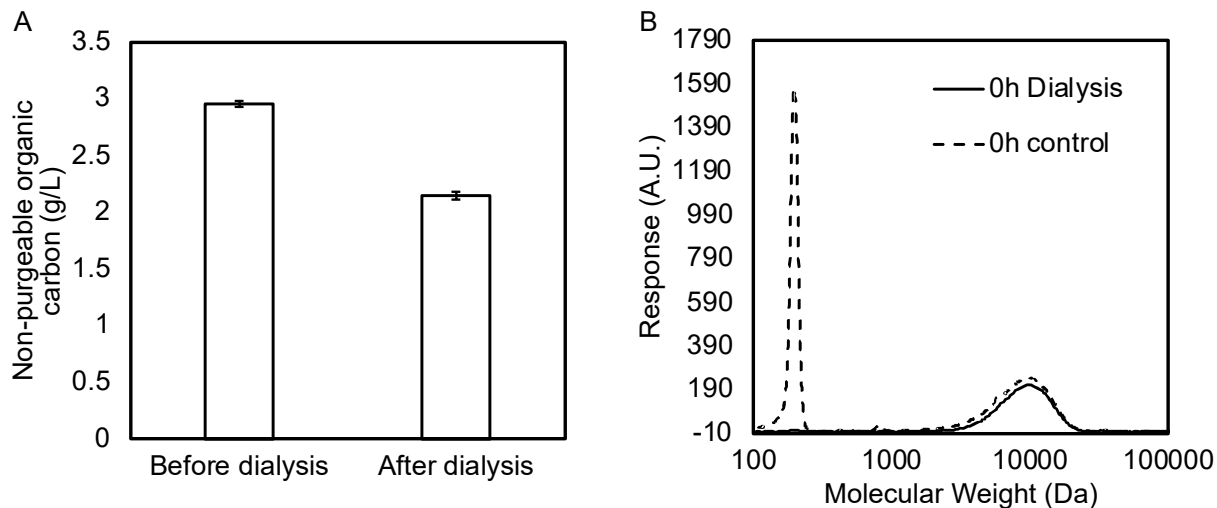
38
39 **Figure S2**. **A)** The TOC measurements of undegraded polymer solution (5 g/L) before (2.96 ±
40 0.03 g/L) and after (2.15 ± 0.04 g/L) dialysis for 72 hours in a 3.6 kDa dialysis bag (27.4%
41 reduction). This reduction cannot be attributed to dilution because the volume in the bag was
42 unchanged before and after dialysis. **B)** The SEC trace of the polymer solution before and after
43 dialysis.

44
45 *Polymer purification via preparative SEC*
46   An identical undegraded polymer solution described above was prepared and injected (30
47 μL) into the SEC column using 0.001 M Na_2SO_4 as mobile phase and a flow rate of 0.5 mL/min.
48 The polymer fraction that was eluted from 5-10 mL was collected as one fraction which
49 corresponded to the SEC peak of the polymer. This fraction was then analyzed on HRMS and
50 analyzed via the stated workflow.
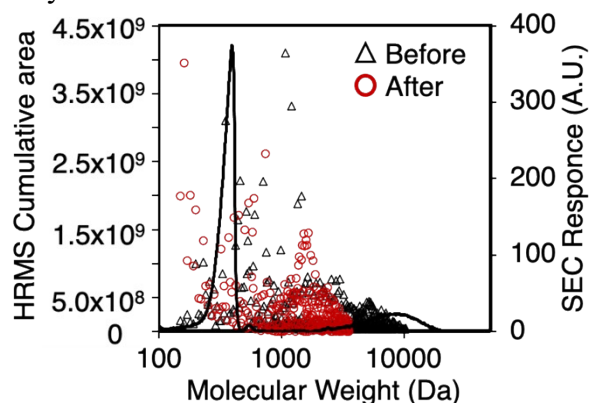
51
52 **Figure S3.** The SEC trace of undegraded and unfractionated polymer (line) and the HRMS profile
53 of the sample before fractionation (black points) and after peak fraction of SEC (red points).
54 Surprisingly, there were still low molecular weight features on HRMS after SEC fractionation.

55

56 *Calculation of HRMS average molecular weight (MW)*
57   The average MW was calculated using the HRMS signal. First, the total area of all the
58 peaks was calculated (i.e., group area, GA). This was then used to calculate the fraction of each
59 peak area at a given MW relative to the total area (i.e., $\dfrac{GA_{MW}}{\sum GA}$).

$$Average\ MW = \sum_{MW} MW \times \frac{GA_{MW}}{\sum GA}$$

60   (**Equation 4**)
61 For the starting polymer, HRMS features with the MW $\geq$ 600 Da were considered in this
62 calculation because it was confirmed that features lower in MW than this were non-polyacrylamide
63 features (observed via manual inspection of features). Note that the accuracy of the measured mass
64 decreases with increasing MW because the resolving power is constant at R=120,000 across
65 different MWs (R = mass/Δmass, where Δmass is a measure of mass accuracy).[1]
66
67 *Hydrolysis analysis of 24h control sample*
68   The 24h control sample was a mixture of polyacrylamide (500 mg/L) at pH 3.5 heated at
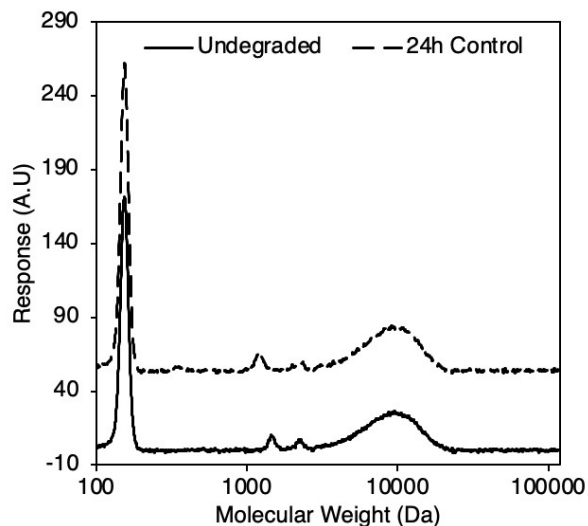69 80°C for 24h without the addition of persulfate.
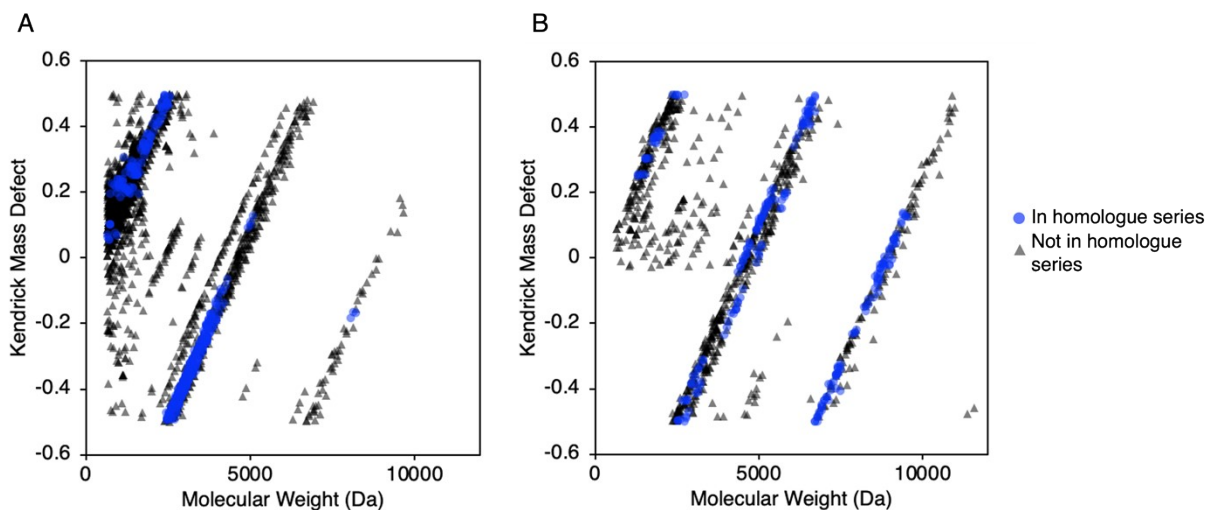
70
71 **Figure S4.** The Kendrick mass defect plots of **A**) undegraded polymer and **B**) the 24h control
72 polymer with acrylic acid ($C_3H_4O_2$) as the Kendrick formula with features in homologue
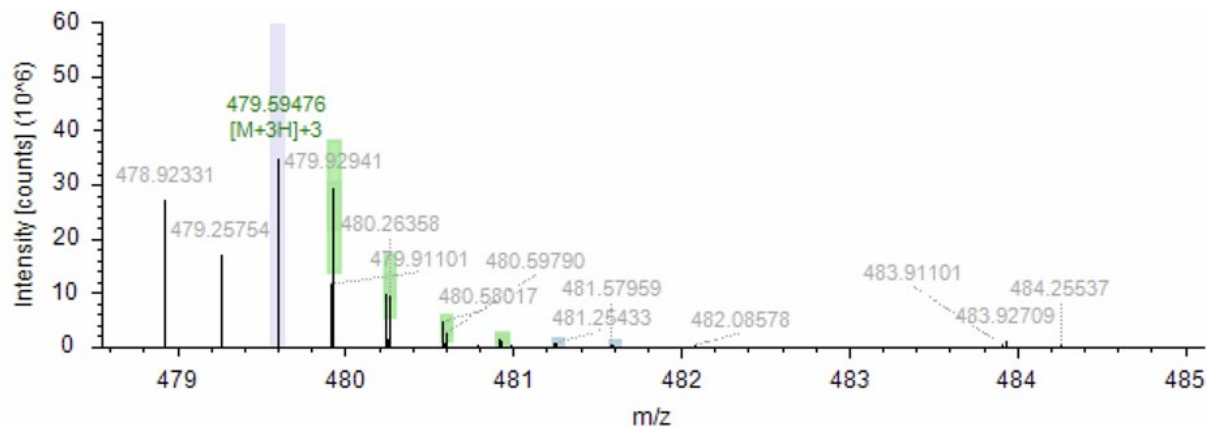73 highlighted in blue.
74
75 According to SEC, we see no molecular weight reduction in our 24h control sample (**Fig. S5**).
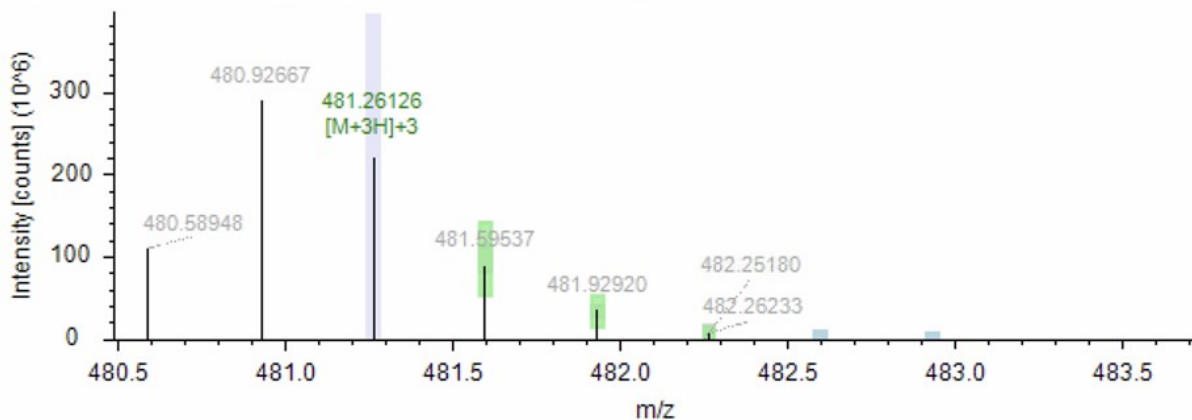
76
77 **Figure S5.** The molecular weight profile of undegraded polymer (solid) and 24h control (dashed)
78 detected by SEC-UV.

79
80 *Example MS¹ spectra showing incorrect monoisotopic peak assignment using the conventional*
81 *nontarget workflow.*

82

83

84
85 **Figure S6.** The MS[1] spectra of features with incorrect monoisotopic peak assignment by
86 conventional workflow using Compound Discoverer. The assigned monoisotopic peak for both

4

87 features (shaded with a light purple bar) had m/z = 479.59476 for top figure and m/z = 481.26126
88 for bottom figure. Both monoisotopic peaks were followed by lower m/z peaks with a Δm/z $\cong$
89 0.333, which indicated these peaks were part of an isotopic pattern of a parent ion with charge +3.
90 Additionally, overlapping peaks in the top spectrum with very close m/z values (i.e.,
91 m/z=479.91101 and 479.92941) in the isotopic pattern may affect the monoisotopic peak
92 assignment (i.e., m/z= 478.92331 is the monoisotopic peak of this feature).
93

94
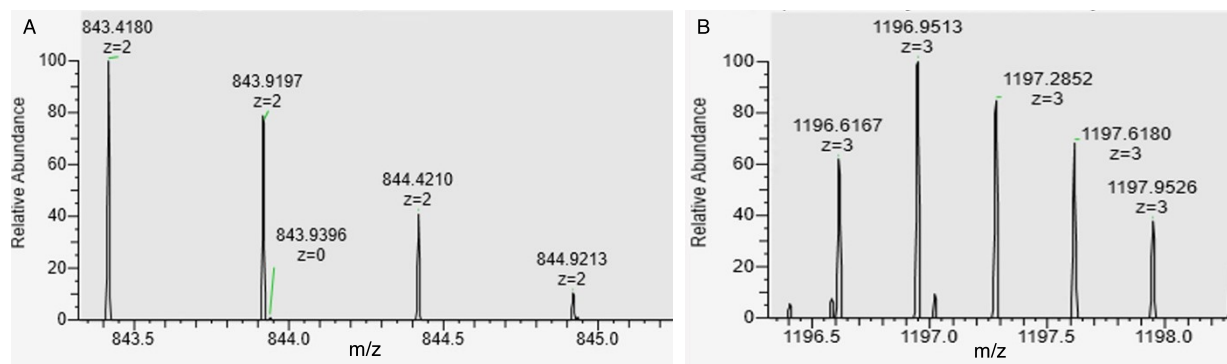
Figure S7. Example spectra of isotopic pattern demonstrating that the monoisotopic peak is not
always the peak with the highest intensity. **A)** isotopic pattern of an accurate mass of 1,688.856
Da, where the monoisotopic peak is the highest intensity peak in the isotopic pattern
(m/z=843.4180), and **B)** isotopic pattern of an accurate mass of 3,592.8801 Da, where the
monoisotopic peak is not the highest intensity peak but rather the peak m/z=1196.6167 in the start
of isotopic pattern.

101

102 *Attempt to resolve monoisotopic peak misassignment by extending LC method.*

103   To better resolve many features eluting between 10 to 25 min, the reverse phase liquid
104 chromatography (RPLC) method was extended from 45 min to 2 h with the same gradient profile.
105 The mobile phase gradient of LC run was set at: 1) 1% B for 5 min at 1 µL/min, 2) then changed
106 to 20% B at 0.20 µL/min over 87.5 min, 3) changed to 95% B at 0.20 µL/min over 17.5 min, and
107 4) finally held at 95% B for 10 min at 1.0 µL/min. Only undegraded polymer was tested. To
108 evaluate if there was an improvement after applying this extended LC method, the modified van
109 Krevelen diagram was created for the newly generated raw features after being processed by the
110 conventional workflow. Only 14.4% of features detected on the extended method was within
111 theoretical limits, comparing to the 21.5% of original LC method. Thus, the extended LC method
112 was not adopted for following study.
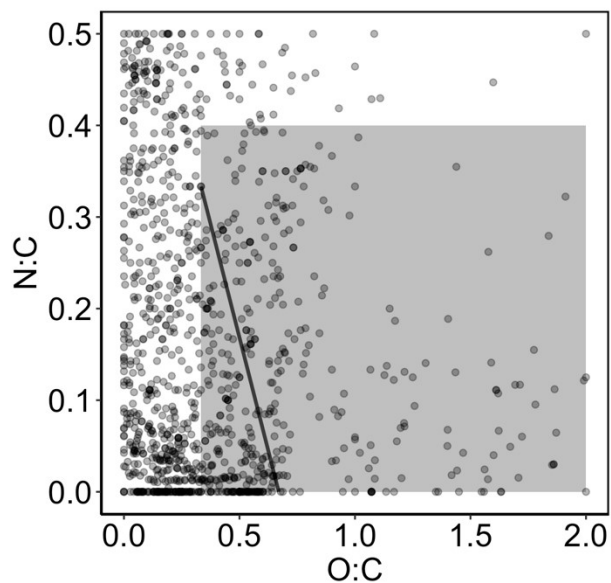
113
Figure S8. The modified van Krevelen diagram for features of undegraded PAM detected using the extended LC method. The shaded area represents the theoretical boundaries of PAM and its degraded products by free radical degradation and hydrolysis. The solid black line represents the hydrolysis products of undegraded polymer. The molecular formulas were predicted directly from the Compound Discoverer software.

119

120 *Summary of detected features.*

121

122 **Table S1.** Summary of the number of features detected in PAM (triplicate) degraded over a specific time. The numbers included features:
123 detected after blank subtraction (Total features detected), detected after peak picking, matched with the newly constructed databases,
124 and matched with compound classes. Additionally, for the database and compound class matches, the number of matches for the given

| Degradation time (hours)	Total features detected	After peak picking	Database matches	Occurrence specific end groups[a]				Compound class matches		
			Total	Methyl or methylene	Aldehyde	Ketone	Carboxylic acid	Total	Aldehyde	Ketone
0	5,605	2,315	259	122	182	161	53	40	37	3
1	9,702	4,790	101	79	53	56	14	548	545	3
5	8,385	5,149	54	58	24	20	6	508	506	2
10	8,794	5,642	87	80	62	25	7	504	502	2
24	4,112	2,655	35	30	25	13	2	152	151	1

125 end group is noted.
126 [a] Every feature contributed two end groups to the total count.

Proposed propagation reaction pathways
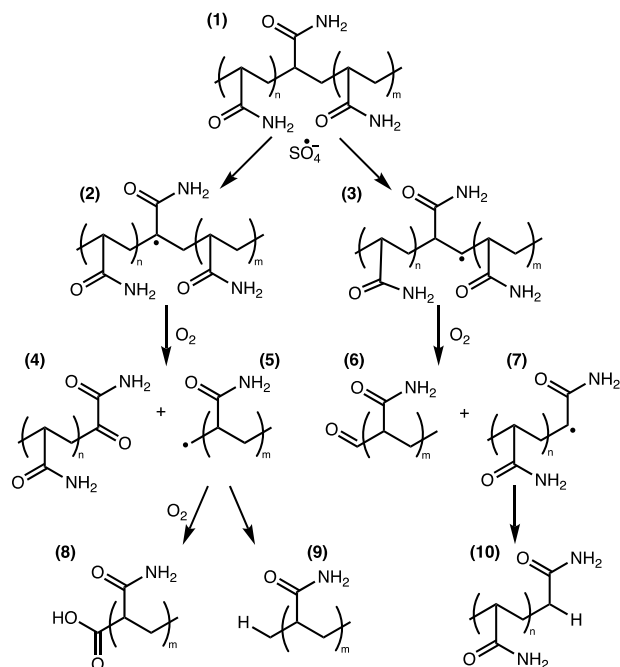
Figure S9. The reaction cascade for the radical induced oxidative chain scission of polyacrylamide (**1**). Sulfate radicals abstract the hydrogen on the tertiary (**2**) or secondary (**3**) carbon on the polymer backbone. In the presence of oxygen, the tertiary carbon radical can produce a ketone terminal group (**4**) and a terminal primary carbon radical (**5**). The secondary radical (**3**), in the presence of oxygen, can produce an aldehyde terminal group (**6**) and another radical on the secondary carbon (**7**).[2,3] These formed radicals (**5** and **7**) can terminate either via abstracting a hydrogen from an adjacent polymer chain (intra- or inter- chain) to form a methyl (**9**) or methylene (**10**) group,[4] or the terminal primary carbon radical (**5**) can react with oxygen and undergo a rearrangement to form carboxylic acid (**8**).[5]

Novel database construction based on previously proposed reaction mechanisms.
The construction of these databases included the following combinations of end groups: aldehyde-aldehyde, aldehyde-ketone, aldehyde-methyl, aldehyde-methylene, aldehyde-carboxylic acid, ketone-ketone, ketone-methyl, ketone-methylene, ketone-carboxylic acid, and methyl-methylene. Focusing on our interest in understanding aldehyde and ketone containing features, only the structures with aldehyde or ketone end groups were further paired with methyl, methylene, and carboxylic acid end groups. We also added methyl–methylene end group pairs because they are the assumed end groups of our starting polymer.

Table S2. The number of unique formulas for a given end group combinations in the constructed databases. The total amount of unique formulas is 463,665.

End Groups	Number of Formula
Aldehyde-aldehyde	29,068
Aldehyde-ketone	57,458
Ketone-ketone	86,190

|	
Aldehyde-methyl	29,068
Aldehyde-methylene	57,460
Aldehyde-carboxylic acid	29,068
Ketone-methyl	29,068
Ketone-methylene	86,190
Ketone-carboxylic acid	57,460
Methyl–methylene	29,068

Aldehyde and Ketone products detected by database matches and abundance calculation.

For each replicate sample at a specific degradation time point, the area measured for each feature was summed across all features that matched with aldehyde or ketone end group formulas in database. The total summed areas for aldehydes and ketones were averaged across triplicate samples at each degradation time point, which was used as the abundance of each end groups. Then their ratio of (i.e., aldehyde/ketone) was reported in **Fig. 4B**. The reported error was properly propagated considering the calculation of the ratio.

Aldehyde and Ketone formation detected by the Compound Class approach.
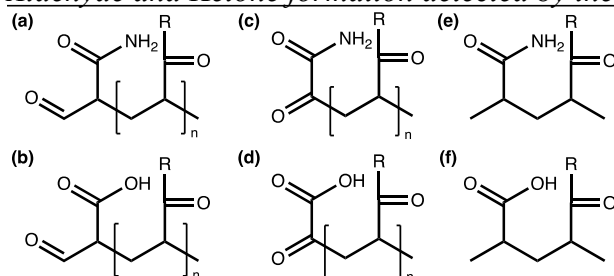
Figure S10. The oligomers used to generate *in silico* fragments for the Compound Class MS^2 databases for aldehyde and ketone detection. The representative structure of **A)** an aldehyde terminal group with an amide side chain and n neighboring monomers of any hydrolysis state, **B)** an aldehyde terminal group with an carboxylic acid side chain and n neighboring monomers of any hydrolysis state, **C)** an ketone terminal group with an amide side chain and n neighboring monomers of any hydrolysis state, **D)** an ketone terminal group with an carboxylic acid side chain and n neighboring monomers of any hydrolysis state, **E)** a two monomer long unit with methyl end groups and at least one amide side chain, and **F)** a two monomer long unit with methyl end groups and at least one carboxylic acid side chain.

Using the Thermofisher MassFrontier software, a terminal group-specific fragment list was generated by *in silico* fragmentation of proposed oligomers containing an aldehyde or a ketone terminal group (**Fig. SI8**). The list of fragments was further selected based upon whether they are unique to aldehyde or ketone end groups, but also are independent of 1) whether the neighboring group contains an amide or carboxylic group and 2) the number of repeating units in the structure (from *n*=1 to 2). To do so, first, structures with only two repeating units (*n*=1) were considered. The list of formulas for structure **(a)** was first compared to a list for ketone end group without hydrolysis **(c)**, and only formulas that were unique for **(a)** were included. The same process was repeated by comparing this generated list with a list for structure **(e).** This updated list was then compared to a formula list from the fragmentation of structure **(a)** where R=OH, and only formulas that were present in both were retained. This updated list was then unique to the fragmentation of structures uniquely with aldehyde end groups, but was independent of hydrolysis

185 of neighboring monomer. Finally, the remaining formulas in this list were compared to a list
186 generated for formulas of **(a)** where n=2 so the list was independent of number of repeating units.
187 The same process was repeated for **(b)** by comparing to **(d)** and **(f)** where the terminal monomer
188 is   hydrolyzed.   A   similar   process   is   repeated   for **(c)** and **(d)** but   comparing
189 to **(a)** and **(b)** respectively in the first step (**Fig. S10**). All comparisons were done directly in a
190 customized R code by comparing the formula of the fragmentation structure (therefore the m/z of
191 the fragments). The lists of compound class were used to flag features with MS^2 spectra that
192 contained one of the listed structures.
193
194 **Table S3**. The formula and structures generated from fragmentation of **aldehyde** end group
195 structures using MassFrontier and were used in Compound Class search. This includes fragments
196 from **Fig S10 a & b**.

Formula	Structure
$C_6H_{11}O_3^+$	
$C_5H_7O_4^+$	
$C_5H_8NO_3^+$	
$C_6H_9O_3^+$	

10

$C_7H_7O_2^+$	[structures]
$C_6H_9O_2^+$	[structure]
$C_6H_7O^+$	[structure]
$C_4H_6NO^+$	[structures]
$C_2H_3O^+$	[structure]

197
198

199 **Table S4.** The formula and structures generated from fragmentation of **ketone** end group
200 structures using MassFrontier and were used in Compound Class search. **Fig S10 c & d.**
201

Formula	Structure
$C_6H_8NO_2^+$	
$C_4H_5O_4^+$	

C₅H₈NO⁺	
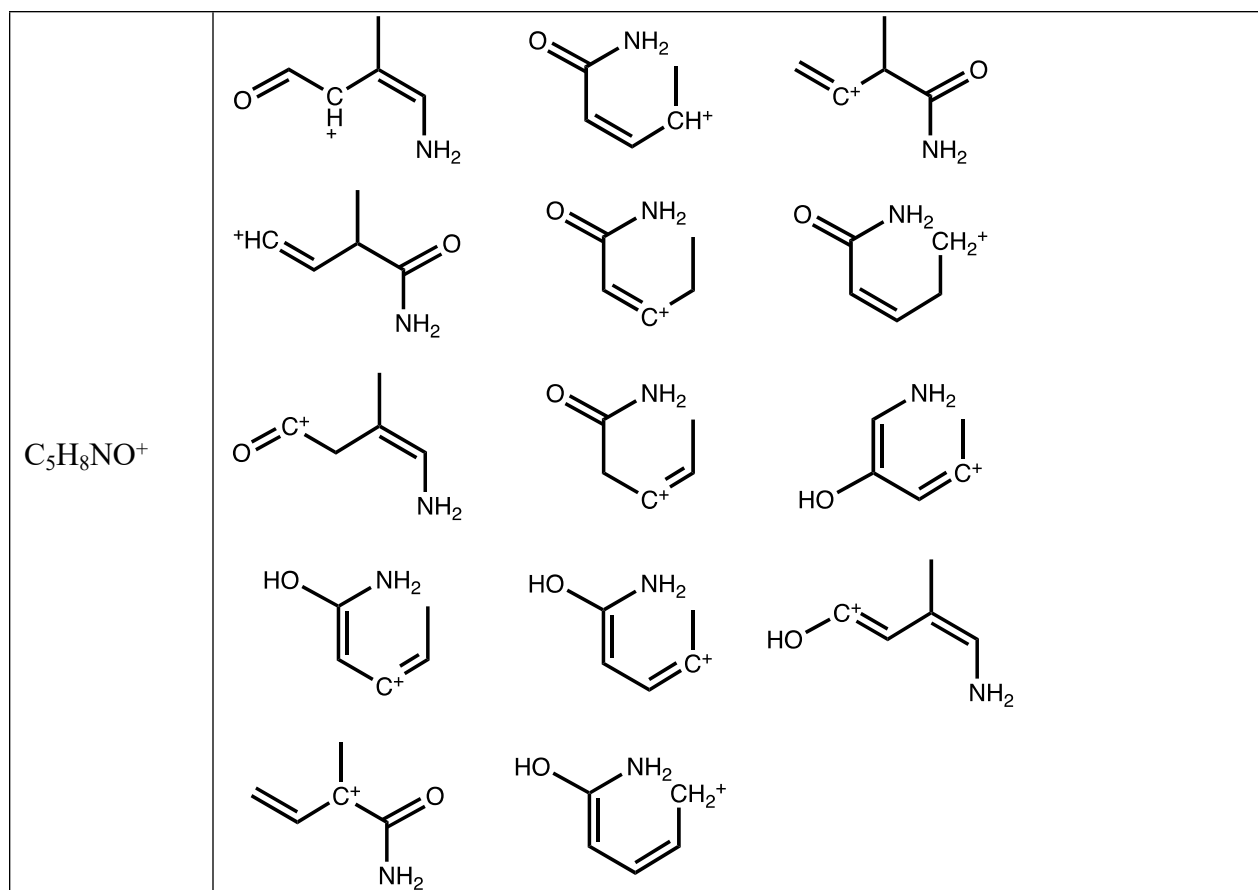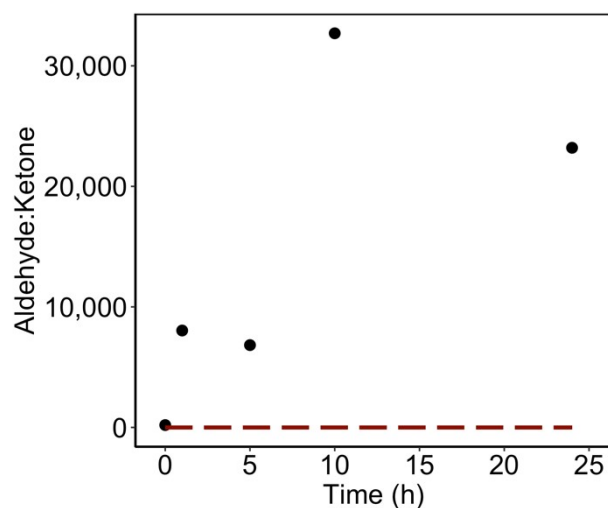
Figure S11. The ratio of total peak area of aldehydes and ketones calculated from all features matched with each compound class. These results showed a similar conclusion regarding the relative abundance of aldehyde to ketone drawn from the application of the novel MS[1] database, however the ratio was significantly higher. The red dashed line represented previously reported ratios of the abundance of carbon centered at secondary versus tertiary carbons for the degradation of polyacrylamide.[6–8]

211

FISh scoring analyses on selected formulas predicted based on matched MS^1 features.

213   The Fragment Ion Search (FISh) score was calculated by comparing the MS^2 spectrum
214 predicted by *in silico* fragmentation to the measured MS^2 spectra of a given proposed parent
215 structure using the Compound Discoverer. The FISh score is the percentage of MS^2 features that
216 matched with the predicted features over the total detected features (**Eqn 5**). FISh score was
217 calculated by applying a high accuracy mass tolerance of 2.5 mmu, a low accuracy mass tolerance
218 of 0.5 Da, and a S/N threshold of 3.

219

$$FISh\ Score = \frac{\#\ of\ matched\ MS^2\ features}{\#\ of\ total\ MS^2\ features\ measured} \times 100 \qquad \textbf{(Equation 5)}$$
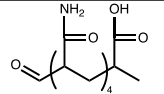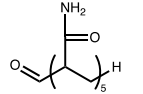
221
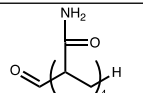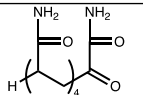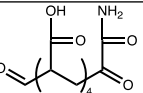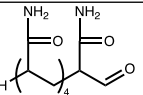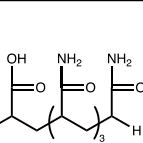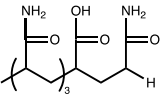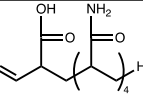
222 **Table S5.** The formula and representative structures used for FISh scoring. For each formula, the
223 structures of all possible isomers were created considering the placement of the amide or
224 carboxylic acid side chains and with the overall restriction of PAM relevant structures. The number
225 of isomers for each generic structure was reported in the Table.

Formula	Generic Structure	Number of Isomers
$C_{13}H_{22}N_4O_5$		1
$C_{14}H_{23}N_5O_6$		5
$C_{15}H_{19}NO_{11}$		5
$C_{15}H_{25}N_4O_7$		1
$C_{15}H_{26}N_4O_6$		5
$C_{15}H_{27}N_5O_5$		1
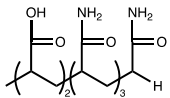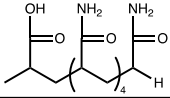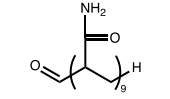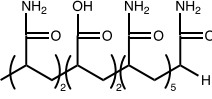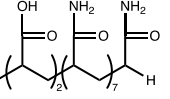
| Formula	Structure	Value
$C_{16}H_{26}N_4O_7$		5
$C_{16}H_{27}N_5O_6$		1
$C_{18}H_{30}N_4O_8$		15
$C_{18}H_{31}N_5O_7$		6
$C_{26}H_{44}N_8O_{11}$		9
$C_{26}H_{43}N_9O_{10}$		1
$C_{28}H_{47}N_9O_{10}$		1
$C_{30}H_{50}N_8O_{12}$		45

226
227

228 **Table S6.** The MS^2 *in silico* fragmentation match results for each structural match. The Compound Discoverer (CD) 3.3 and MetFrag
229 web-based software results are included for each feature. For CD, the top structure match is reported, as well as the matched fragments
230 between the detected fragments on MS^2 and the *in silico* fragments predicted for that structure. The FISh score is reported for each
231 structural match. For MetFrag, the structural match is reported if it is different from the top match according to CD. The matched
232 fragments according to MetFrag are also listed, and the raw MetFrag score is reported for each match. When the top structure is the
233 same for each software, the fragments that are commonly matched in both software are highlighted in green, and the total number is
234 listed. When the top structural matches are different, this information is not included. Finally, the Schymanski level of confidence match
235 is reported for each feature.

| Formula | Compound Discoverer | | | MetFrag | | | Number of common fragments | Level of Match |
	Structure Match	Matched Fragments	FISh Score	Structure Match (if different from CD)	Matched Fragments	MetFrag Score		
$C_{13}H_{22}N_4O_5$		73.02766, 59.0485	25		86.04681	1.8517	0	3a
$C_{14}H_{23}N_5O_6$		59.04853, 69.0326, 217.01617	13.33		59.04853, 73.02766	7.9931	1	3b
$C_{15}H_{19}NO_{11}$		281.06470, 337.05777	22.22		140.03326	11.6851	0	3b
$C_{15}H_{25}N_5O_6$		73.02733, 111.04287, 115.0862	16.67		73.02733, 87.04317, 115.08627	20.1398	2	3b
$C_{15}H_{26}N_4O_6$		59.04833, 69.03239, 73.02747, 73.06451, 86.03547, 87.04311, 89.05870, 95.04831, 99.04323, 103.07465, 113.05862, 129.05313, 131.06931	46.43		69.03239, 73.02747, 86.03547, 87.04311, 99.04323, 101.05865, 129.05313, 217.10741, 219.1217	38.4583		3a
$C_{16}H_{26}N_4O_7$		73.0276, 87.04321, 89.05924	75		73.0276, 87.04321	23.943		3a
$C_{16}H_{27}N_5O_6$		73.02764, 283.17529	25		73.02764, 87.04327, 283.17529, 351.16748	65.4826	2	2b

16

| Formula	Structure	Fragments	Value	Structure	Fragments	Value		
$C_{18}H_{30}N_4O_8$		84.08051, 87.04317, 89.05883, 99.04305, 113.05898, 115.08568, 129.10156, 131.06981, 133.08522, 175.09659	40		87.04317, 99.04305, 113.05898, 115.08568, 129.10156, 131.06981	36.0594	6	2b
$C_{18}H_{31}N_5O_7$		73.0276, 87.04319, 89.05886	62.5		73.02771, 87.04341, 89.05927	27.9099	2	2b
$C_{28}H_{47}N_9O_{10}$		89.05862, 102.05399, 129.10135, 200.09380, 653.31519	10.64		102.05399, 129.10135, 257.13626, 513.25439, 539.30359, 609.30963, 653.31519	380.2097	3	3b
$C_{30}H_{50}N_8O_{12}$		73.02708, 84.04314, 87.04288, 102.05360, 115.08513, 129.10075, 201.12315, 211.10606, 216.08656, 243.07901, 426.18860, 554.28259, 582.27661, 583.27380, 597.28674	18.29		73.02708, 84.04314, 87.04288, 115.08513, 129.10075, 198.07576, 201.12315, 216.08656, 243.13409, 398.18976, 410.19006, 425.19083, 426.1886, 537.25537, 554.28259, 555.29187, 581.27814, 597.28674, 697.35425	192.1527		3b

237   **Fig. S12-23** showed examples of FISh scoring analysis for results with a FISh score >10.
238 The green colored features represent features matched with the *in silico* fragmentation spectra.
239 Only features the with the highest scores for each feature were listed in **Fig. S24**.
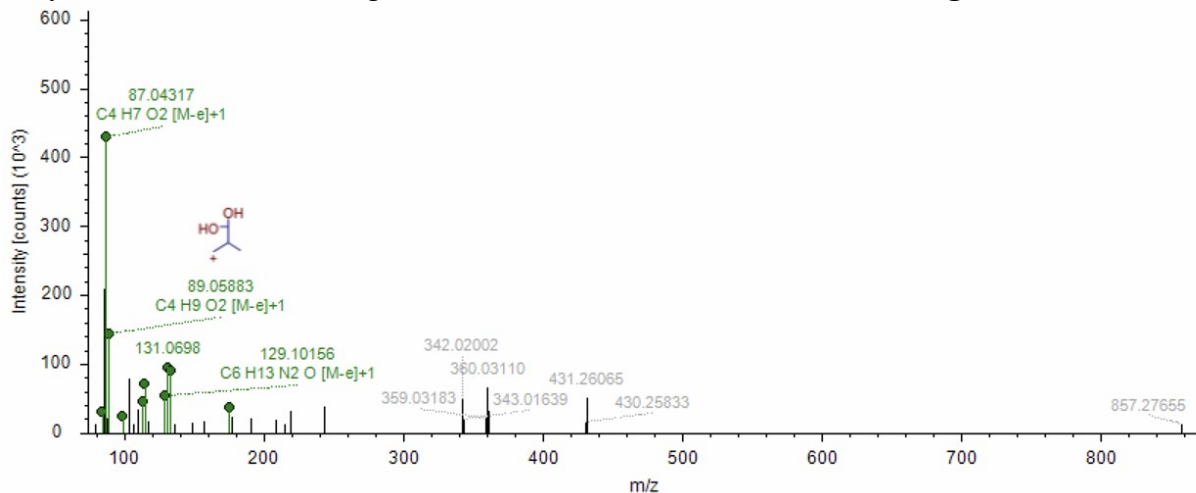
240
241 **Figure S12.** The MS^2 spectra of formula $C_{18}H_{30}N_4O_8$ whose structure was shown in **Fig. 5A.** The
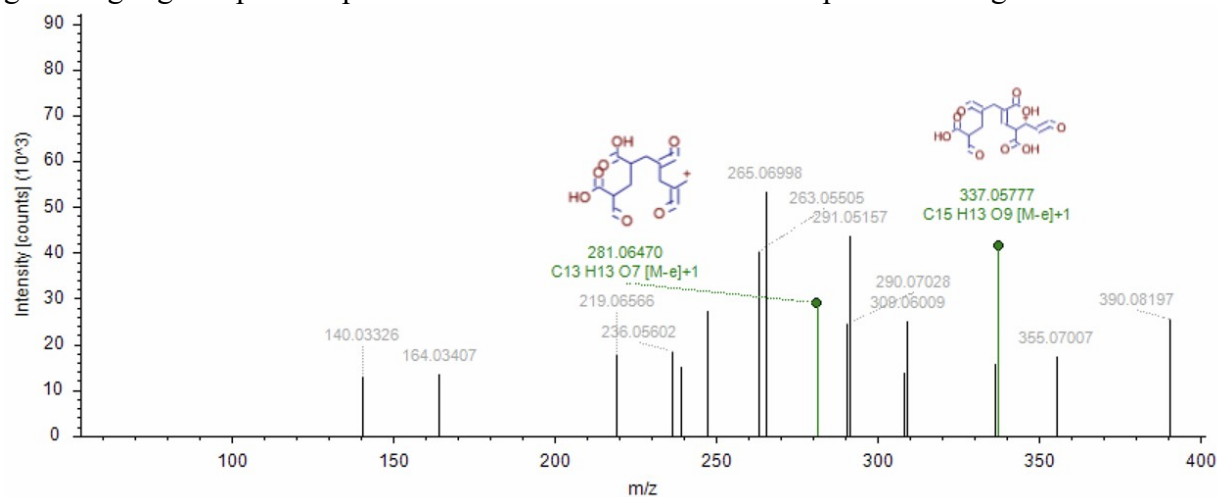242 green highlighted peaks represent matches with the theoretical spectra of the given structure.
243
244
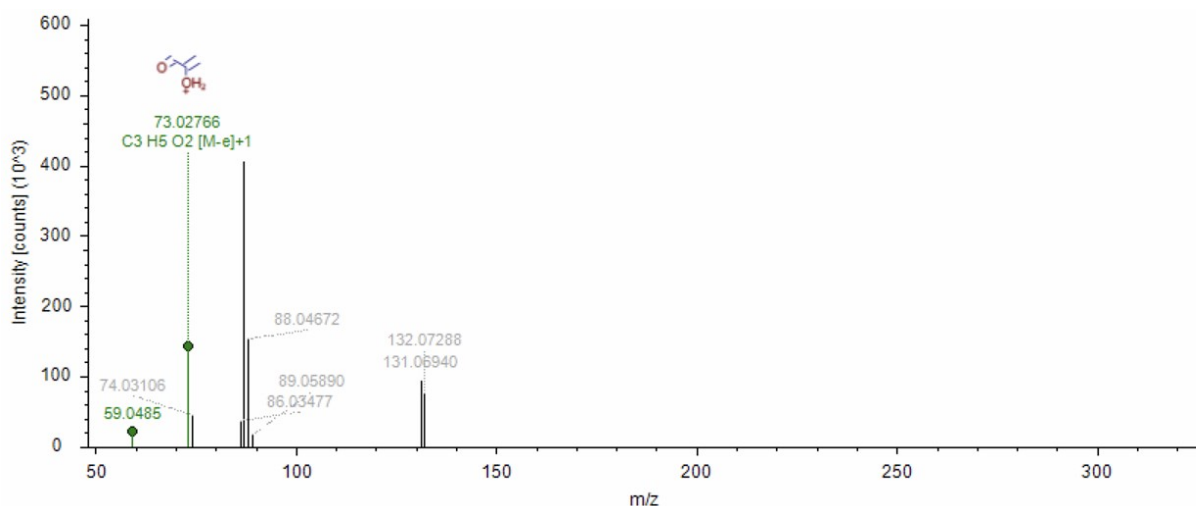
245
246 **Figure S13.** The MS^2 spectra of formula $C_{13}H_{22}N_4O_5$ whose structure was shown in **Fig. 5B.** The
247 green highlighted peaks represent matches with the theoretical spectra of the given structure.
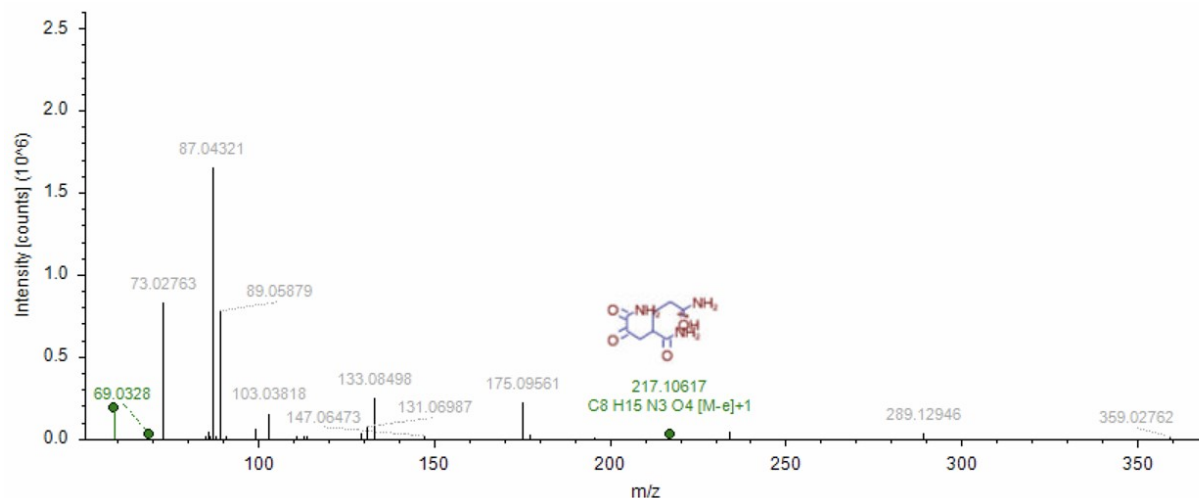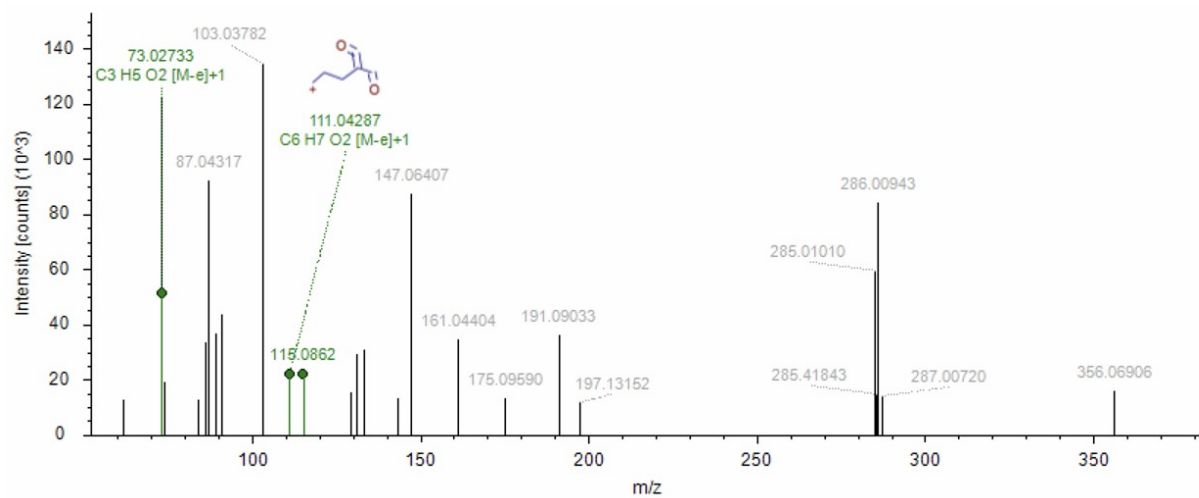
248
249 **Figure S14.** The MS^2 spectra of formula $C_{14}H_{23}N_5O_6$ whose structure was shown in **Fig. 5C.** The
250 green highlighted peaks represent matches with the theoretical spectra of the given structure.
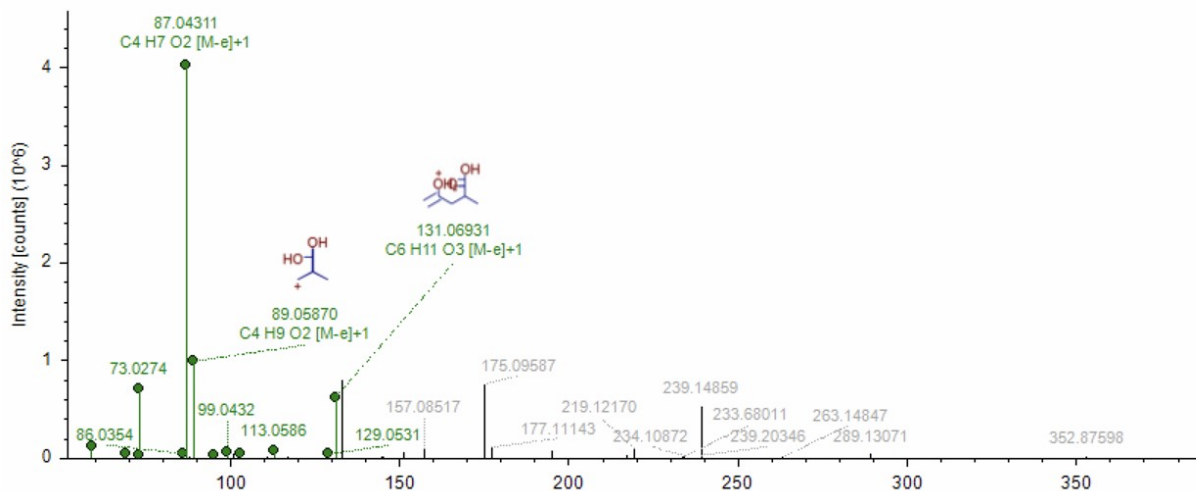

251
252 **Figure S15.** The MS^2 spectra of formula $C_{15}H_{19}NO_{11}$ whose structure was shown in **Fig. S23A.**
253 The green highlighted peaks represent matches with the theoretical spectra of the given structure.
254

255

256 **Figure S16.** The MS^2 spectra of formula $C_{15}H_{25}N_5O_6$ whose structure was shown in **Fig. S23B.**
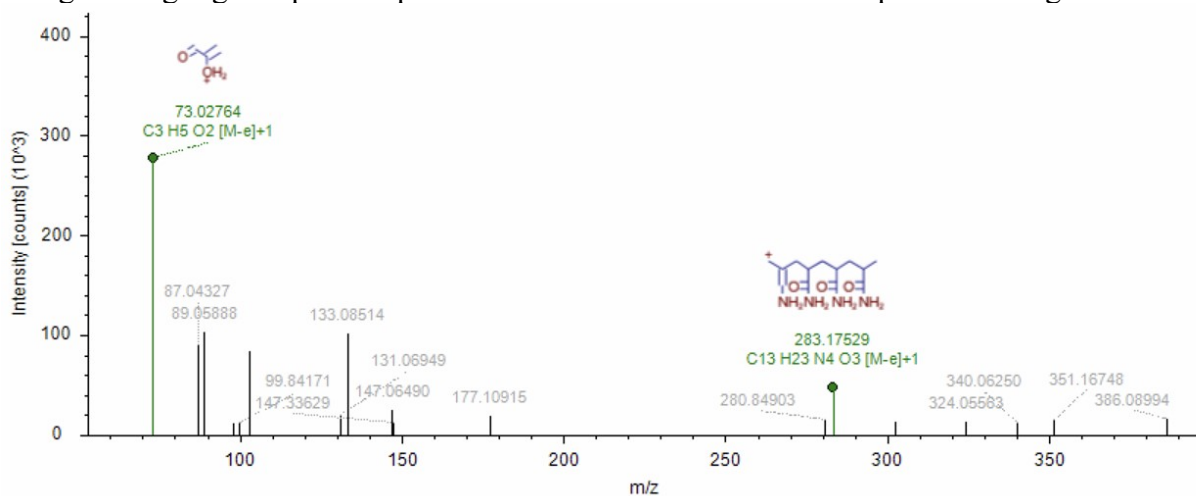257 The green highlighted peaks represent matches with the theoretical spectra of the given structure.
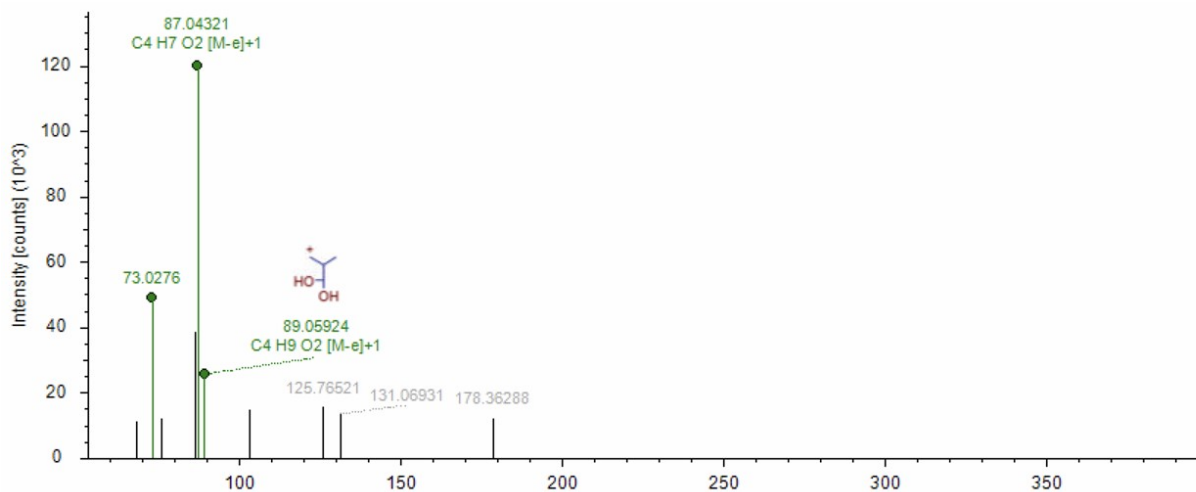258

259
260 **Figure S17.** The MS^2 spectra of formula $C_{15}H_{26}N_4O_6$ whose structure was shown in **Fig. S23C.**
261 The green highlighted peaks represent matches with the theoretical spectra of the given structure.

262
263 **Figure S18.** The MS^2 spectra of formula $C_{16}H_{27}N_5O_6$ whose structure was shown in **Fig. S23D.**
264 The green highlighted peaks represent matches with the theoretical spectra of the given structure.
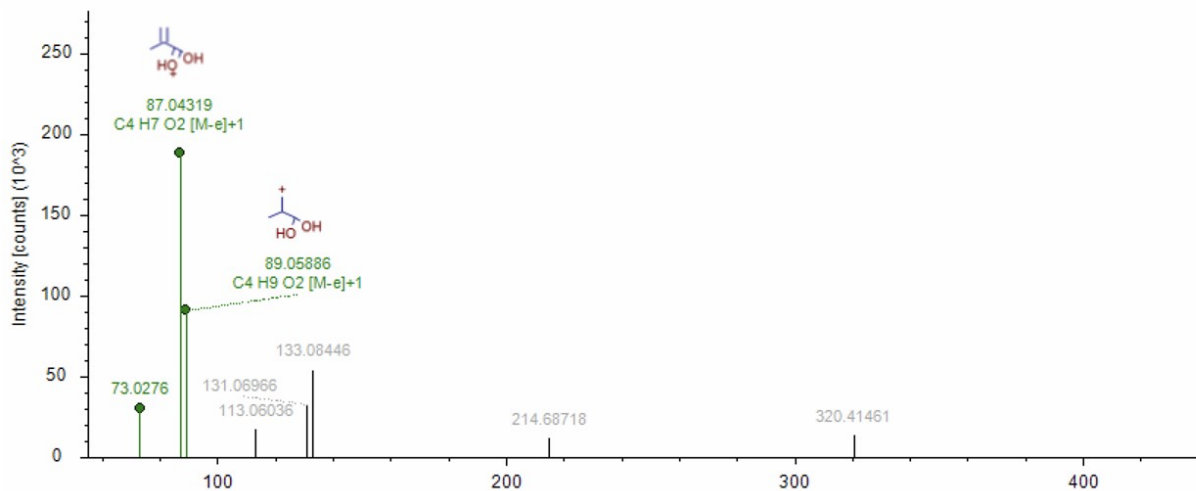265

266
267 **Figure S19.** The MS^2 spectra of formula $C_{16}H_{26}N_4O_7$ whose structure was shown in **Fig. S23E.**
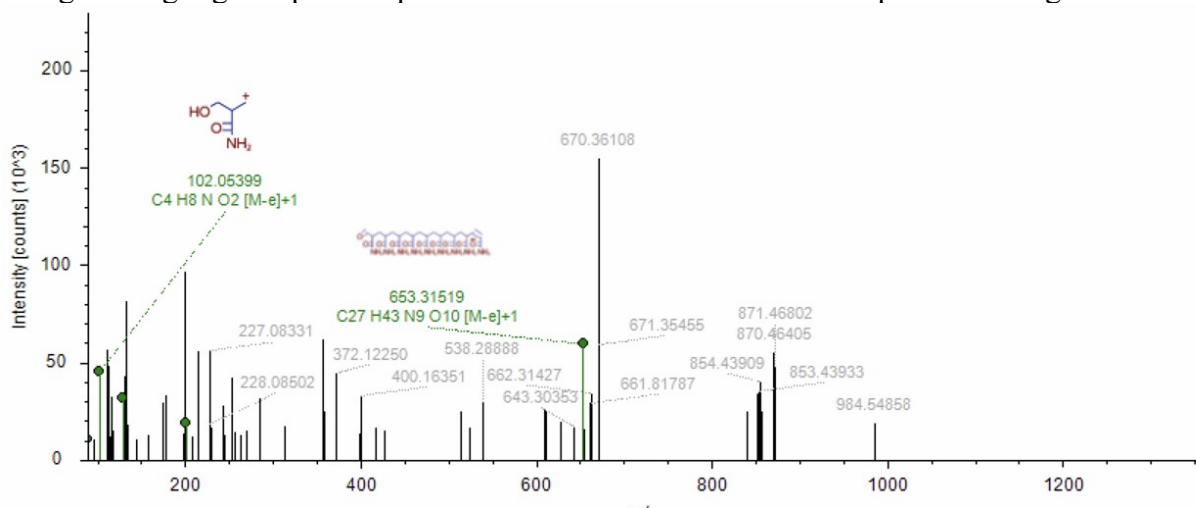268 The green highlighted peaks represent matches with the theoretical spectra of the given structure.
269

270
271 **Figure S20.** The MS^2 spectra of formula $C_{18}H_{31}N_5O_7$ whose structure was shown in **Fig. S23F.**
272 The green highlighted peaks represent matches with the theoretical spectra of the given structure.

273

21

274 **Figure S21.** The MS^2 spectra of formula $C_{28}H_{47}N_9O_{10}$ whose structure was shown in **Fig. S23G.**
275 The green highlighted peaks represent matches with the theoretical spectra of the given structure.

276
277
278 **Figure S22**. The MS^2 spectra of formula $C_{30}H_{50}N_8O_{12}$ whose structure was shown in **Fig. S23H.**
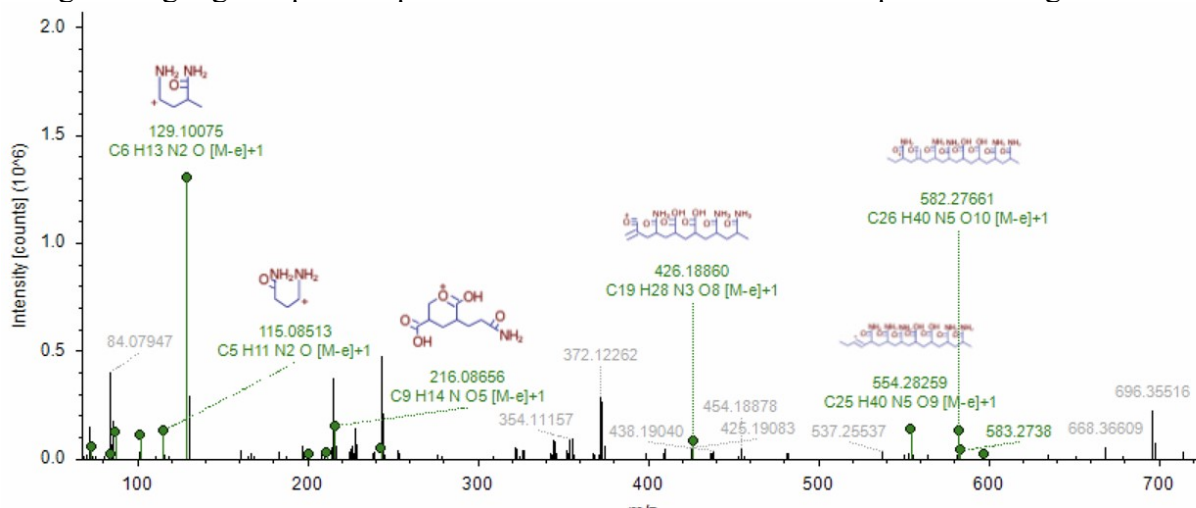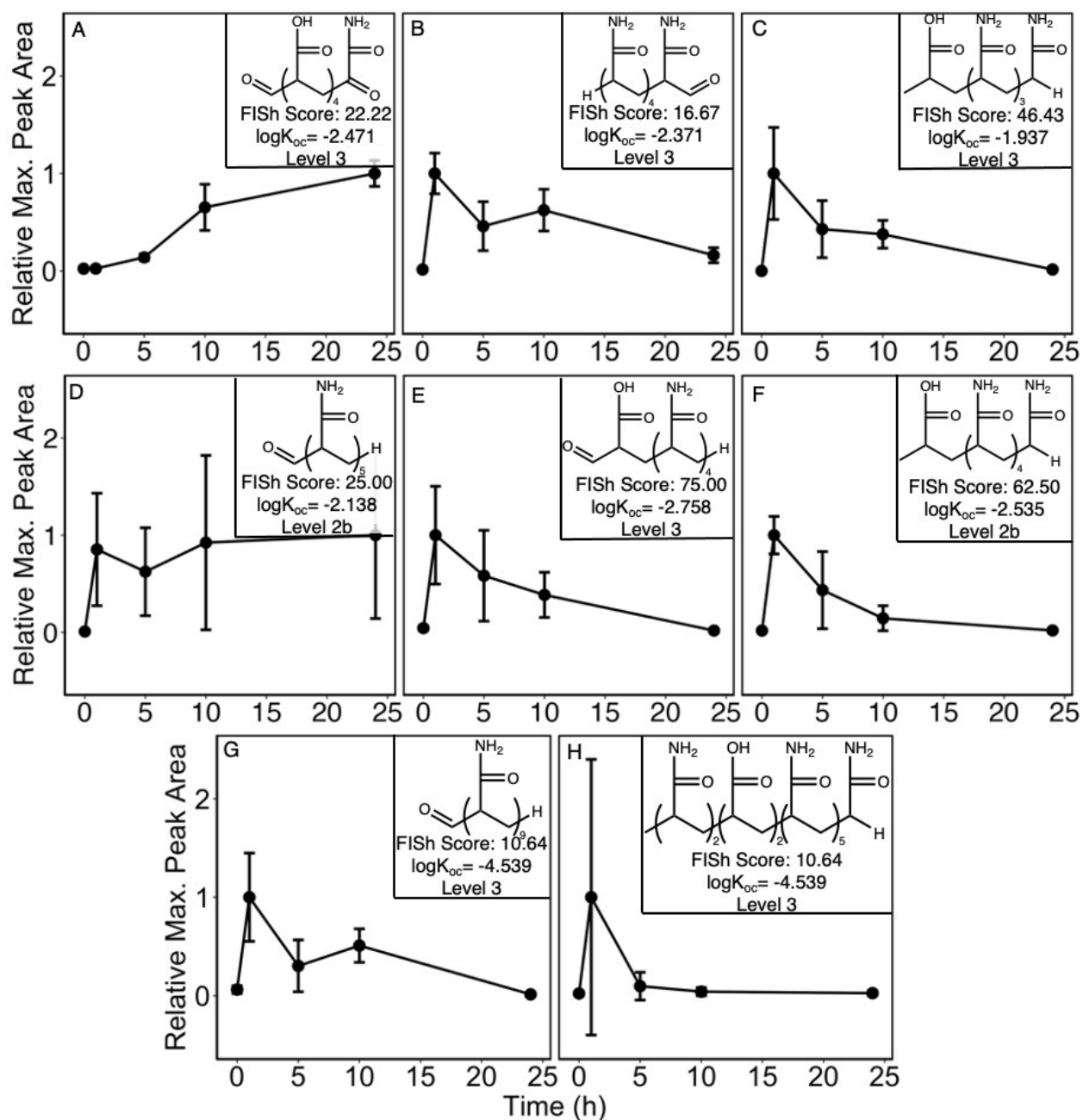279 The green highlighted peaks represent matches with the theoretical spectra of the given structure.
280

Figure S23. The peak area of feature matches relative to the maximum peak area of feature in each sample variation over time. These features were selected due to their high FISh score. The inset box included structure, FISh score, calculated $logK_{oc}$ on EPISuite software, and the Schymanski level of confidence for nontarget analysis.[9] The error bars represented the standard deviation between triplicate samples at each time point. **A)** A 5-repeating unit oligomer with aldehyde and ketone terminal groups and four acrylate monomers was determined as a level 3 confidence match. **B)** This 5- repeating unit oligomer with aldehyde and methylene terminal groups and no acrylate monomers was determined as a level 3 confidence match. **C)** This 5-repeating unit oligomer with methyl and methylene terminal groups and one acrylate monomer was determined as a level 3 confidence. **D)** This 5-repeating unit oligomer with methyl and aldehyde terminal groups and no acrylate monomers was determined as a level 2b confidence match. **E)** A 5-repeating unit oligomer

23

293 with aldehyde and methyl terminal groups and one acrylate monomer was determined as a level 3
294 confidence match. **F)** This 6-repeating unit oligomer with methyl and methylene terminal groups
295 and one acrylate monomer was determined as a level 2b confidence match. **G)** This 9-repeating
296 unit oligomer with methyl and aldehyde terminal groups and acrylate monomers was determined
297 as a level 3 confidence match. **H)** This 10-repeating unit oligomer with methyl and methylene
298 terminal groups and two acrylate monomers was determined as a level 3 confidence match. The
299 abundance of **A** feature relative to all other features in the sample increased over 24 h; the
300 abundance of all other features remained constant or declined over 24 h.

References

1   K. De Bruycker, A. Welle, S. Hirth, S. J. Blanksby and C. Barner-Kowollik, Mass spectrometry as a tool to advance polymer science, *Nat Rev Chem*, 2020, **4**, 257–268.

2   B. Xiong, R. D. Loss, D. Shields, T. Pawlik, R. Hochreiter, A. L. Zydney and M. Kumar, Polyacrylamide degradation and its implications in environmental systems, *NPJ Clean Water*, 2018, **1**, 17.

3   B. Xiong, Z. Miller, S. Roman-White, T. Tasker, B. Farina, B. Piechowicz, W. D. Burgos, P. Joshi, L. Zhu, C. A. Gorski, A. L. Zydney and M. Kumar, Chemical Degradation of Polyacrylamide during Hydraulic Fracturing, *Environ Sci Technol*, 2018, **52**, 327–336.

4   D. Griller and K. U. Ingold, Persistent Carbon-Centered Radicals, *Acc Chem Res*, 1976, **9**, 13–19.

5   L. Costa, M. P. Luda and L. Trossarelli, Ultra high molecular weight polyethylene - II. Thermal-and photo-oxidation, *Polym Degrad Stab*, 1997, **58**, 41–54.

6   N. N. Lichtin, Selectivity in fast reactions of aqueous OH-radicals with amides, *Isr J Chem*, 1971, **9**, 397–403.

7   U. Grollmann and W. Schnabel, Free radical-induced oxidative degradation of polyacrylamide in aqueous solution, *Polym Degrad Stab*, 1982, **4**, 203–212.

8   J. Suzuki, H. Harada and S. Suzuki, Ozone treatment of water-soluble polymers. V. ultraviolet irradiation effects on the ozonization of polyacrylamide, *J Appl Polym Sci*, 1979, **24**, 999–1006.

9   E. L. Schymanski, J. Jeon, R. Gulde, K. Fenner, M. Ruff, H. P. Singer and J. Hollender, Identifying small molecules via high resolution mass spectrometry: Communicating confidence, *Environ Sci Technol*, 2014, **48**, 2097–2098.

327